Modeling Impact on a One-Link Flexible Robotic Arm

B. V. Chapnik, G. R. Heppler, and J. D. Aplevich

Abstract—**A finite-element model of a single-link flexible robotic arm including the effects of beam damping, hub inertia, and both Coulomb and viscous hub friction is derived. The initial conditions required to represent impact loading are determined, and the motion of the arm under impact loading is simulated. Simulation results are compared to experimental data.**

I. Introduction

FLEXIBLE beams have been a topic of investigation in the robotics field since the early 1970's [1]. They have been used to model the flexibility in robotic members, a phenomenon that has gained in importance as a result of a widespread attempt to lighten robotic assemblies for increased speed and efficiency.

Flexible robot members have frequently been modeled analytically, using Bernoulli-Euler [2]-[6] or Timoshenko [7], [8] beam models. These models have also been incorporated into finite-element representations of the type described here [9]-[11]. More general methods for modeling all possible physical phenomena associated with elastic body dynamics [12]-[15] are also of interest. Most investigators, however, consider only the response of flexible beams to hub-actuated torque, the prevalent condition in robotic control applications.

What if we wish to investigate a flexible robotic arm that has been subjected to an impact at its tip? For example, we may wish to build a flexible robotic arm to catch a baseball, play tennis, snatch a stationary object from a table, hammer a nail into a board, or to collect space debris while attached to a moving space vehicle. To model the effects of these actions on the flexible arm, the impact dynamics of flexible beams must be examined. While many dynamicists have investigated the flexible-beam impact problem for simply supported beams impacted in the center [7], [8], [16]-[18], none have examined the tip impact of a flexible beam attached at its base to a rotor that has friction and inertia, conditions that are of fundamental importance to the modeling of the motions described above.

This paper describes a finite-element model of a flexible beam attached to a rotor that has friction and inertia. The finite-element method is used because it simplifies the inclusion of initial conditions such as those generated by tip impact, hub-applied torques, and frictional torques. Coulomb friction is incorporated into the formulation, including slip-stick characteristics. Rayleigh beam damping and viscous hub friction are also considered.

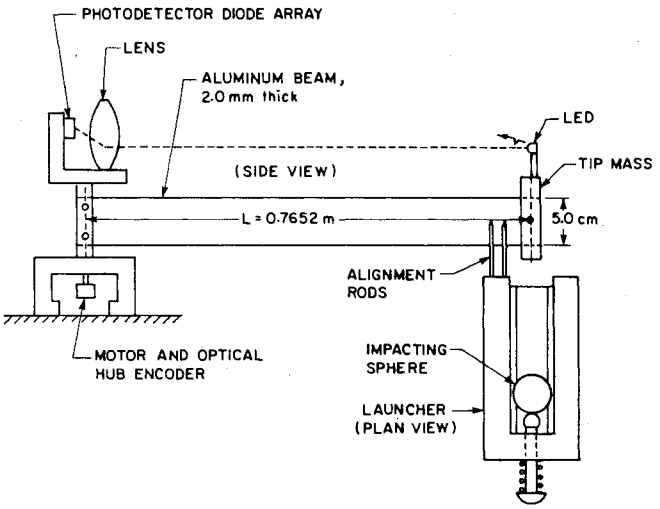

Fig. 1. Experimental apparatus.

Numerical results generated by the model are compared to experimental data gathered from a single-link flexible arm apparatus in the Department of Electrical Engineering at the University of Waterloo [19], [20]. Through this experimental data, it will be shown that the derived model accurately predicts both impact effects and the ensuing motion of the flexible arm.

II. Experiment Description

The basis for the experiment is a one-link flexible arm [19], [20], which consists of a long, thin, deep aluminum beam clamped at one end of the shaft of a direct-drive motor. Affixed to the free end of the beam is a slotted steel cylinder, mounted symmetrically across the neutral axis of the beam to avoid torsional effects. The slot in the tip mass allows its mass center to be aligned with the beam tip. A diagram of this apparatus is shown in Fig. 1.

A lead ball is launched from a spring-loaded ramp to impact the center of the tip mass. The ramp is aligned so that the sphere strikes the tip mass along a line that intersects and is perpendicular to the neutral axis of the beam and is also perpendicular to the hub axis. The ramp alignment also

Manuscript received September 12, 1989; revised December 18, 1990.

B. V. Chapnik is with Vibron Limited, Mississauga, Ont., Canada L5T 1A3.

G. R. Heppler is with the Department of Systems Design Engineering, University of Waterloo, Waterloo, Ont., Canada N2L 3G1.

J. D. Aplevich is with the Department of Electrical Engineering, University of Waterloo, Waterloo, Ont., Canada N2L 3G1.

IEEE Log Number 9100095.

1042-296X/91/0800-0479$01.00

ensures that the sphere is close to the peak of its trajectory upon impact (i.e., its motion is horizontal). The velocity of the sphere as it leaves the ramp is measured using two closely placed photoemitter/detector pairs.

Tip deflection is measured from a line that is tangent to the beam at the hub by using a light beam from a powerful LED fastened to the top of the tip mass, focused through a hub-mounted lens assembly onto a photodetector diode array [19], [21]. Hub deflection is measured using an optical hub angle encoder with a resolution of 4800 counts per revolution.

III. Finite-Element Model

This section describes the formulation of a finite-element model of a flexible beam attached to a rotor with both friction and inertia.

The experimental configuration was designed to eliminate the possibility of torsion of the beam; hence, torsion effects have not been included in the model. Because the beam is long and slender, transverse shear and rotary inertia effects may be neglected. This allows the use of the Bernoulli–Euler beam theory to model the elastic behavior of the arm. In the event that the beam was shorter and thicker, it would be necessary to include transverse shear and rotary inertia effects by using the Timoshenko beam theory rather than the Bernoulli–Euler beam theory. Axial tension and compression effects are minimal and may be neglected because the centripital accelerations in the experiment are very low. Gravity is assumed to be negligible because the beam is thin compared to its depth, and the motion of the beam is confined to the horizontal plane (see Fig. 1). Consequently, the in-plane deflections will be much more significant than the out-of-plane deformations due to gravity. In addition, because the principal axes of the beam cross section lie in and are perpendicular to the plane of rotation, there will be no coupling between the deflections in and out of the plane. Each finite element is considered to have constant cross section and uniform material properties throughout.

Proportional damping in the beam material has been assumed because this common and versatile damping model has the advantage that the frequencies and mode shapes are identical in both the damped formulation and the undamped formulation, providing a significant computational advantage. Another advantage is that this damping model allows experimentally determined damping ratios of individual modes to be used directly in forming the global damping matrix. It also allows the assignment of individual damping ratios to individual modes, such that the total beam damping is the sum of the damping in the modes. Finally, the assumption results in a model that is a good representation of the actual behavior of the beam.

Given the above assumptions, the model has been formulated in a general fashion, making use of the Bernoulli–Euler theory because of the extreme slenderness of the beam. The simulation (see Section VII) makes use of experimentally determined values for the parameters.

The beam is considered to be clamped to a rotating hub, and its motion in the global frame is expressed by two components: a "rigid-body" component describing the motion of a line that is tangent to the beam at the hub (to be referred to as the rigid-body line) and a component describing the elastic deflection of the beam from this tangent line (see Fig. 2). The position of any point on the beam is given (for small $w(x, t)$) by

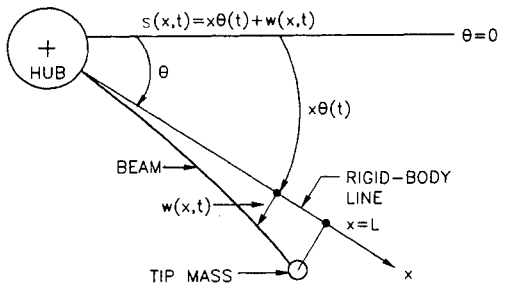

Fig. 2. Frame of reference.

$$S = x\Theta + w(x, t) \tag{1}$$

where x is the distance along the undeformed beam. The elastic deflection $w(x, t)$ is to be approximated using finite-element techniques.

The following sections outline the steps required to build a finite-element model that will approximate the process under investigation.

A. Element Basis Functions

The beam is approximated by partitioning it into N finite elements. As a consequence of using the Bernoulli–Euler beam theory, the finite-element method requires that, for an element with nodes only at its ends, each node possess two degrees of freedom, a transverse deflection and a rotation, which in turn necessitates the use of cubic basis functions. The usual Hermite cubic basis functions for the local interval [0, 1] are used such that the element shape functions are given by

$$\begin{aligned}\phi_1(s) &= 1 - 3s^2 + 2s^3\\ \phi_2(s) &= l_n(s - 2s^2 + s^3)\\ \phi_3(s) &= 3s^2 - 2s^3\\ \phi_4(s) &= l_n(s^3 - s^2).\end{aligned} \tag{2}$$

The local coordinate s is related to the beam coordinate x by using the linear transformation for element n

$$x = x_{n-1} + l_n s. \tag{3}$$

This transformation allows the transverse deflection for the nth element to be expressed in the form [11]

$$w_n(s, t) = [\Phi]_n\{Q\}_n \tag{4}$$

where $[\Phi]_n = [\phi_1(s), \phi_2(s), \phi_3(s), \phi_4(s)]_n$ and $\{Q\}_n = [w_{n-1}(t), \theta_{n-1}(t), w_n(t), \theta_n(t)]^T$. The notation $[\cdot]$ indicates a matrix while the notation $\{\cdot\}$ indicates a vector. In this equation, $w_{n-1}(t)$ and $w_n(t)$ are the elastic deflections of the nodes the ends of the element, and $\theta_{n-1}(t) = w_{n-1,x}(t)$ and $\theta_n(t) = w_{n,x}(t)$ are the corresponding rotations, where $(\cdot)_{,x}$ indicates partial differentiation with respect to x.

B. Global Dynamic Equations

The semidiscretized equations of motion for the flexible arm system can be expressed as

$$[M]\{\ddot{Q}\} + [C]\{\dot{Q}\} + [K]\{Q\} = \{F\} \qquad (5)$$

where $[M]$, $[C]$, and $[K]$ are the global mass, damping, and stiffness matrices, respectively, $\{F\}$ is the external force vector (applied torque is specified in the first entry of this vector), and $\{Q\} = [\Theta, w_0, \theta_0, w_1, \theta_1, \cdots, w_N, \theta_N]^T$.

These equations of motion can be obtained by applying the Euler–Lagrange equations, given by

$$\frac{d}{dt}\left(\frac{\partial \mathcal{L}}{\partial \dot{q}_i}\right) - \frac{\partial \mathcal{L}}{\partial q_i} = 0, \qquad i = 1, \cdots n \qquad (6)$$

where q_i are the generalized coordinates of the model and $\mathcal{L} = T - V$ is the Lagrangian. T is the kinetic energy of the system and V is the total potential energy given by $V = U - W$, where U is the strain energy in the beam and W is the external work done on the beam. The Lagrangian is given by the following expression:

$$\mathcal{L} = \frac{1}{2}\int_L \rho A \dot{S}^2\, dx + \frac{1}{2} m_T \left(L\dot{\Theta} + \dot{w}\,|_{x=L}\right)^2 + \frac{1}{2} J_H \dot{\Theta}^2 - \frac{1}{2}\int_L EI\left(\frac{d^2 w}{dx^2}\right)^2 dx + W. \qquad (7)$$

By substituting for S from (1), the Lagrangian may be reexpressed as

$$\mathcal{L} = \frac{1}{2}\int_L \rho A x^2 \dot{\Theta}^2\, dx + \int_L \rho A x \dot{\Theta}\dot{w}\, dx + \frac{1}{2}\int_L \rho A \dot{w}^2\, dx + \frac{1}{2} m_T L^2 \dot{\Theta}^2 + m_T L \dot{\Theta}\dot{w}\,|_{x=L} + \frac{1}{2} m_T (\dot{w}\,|_{x=L})^2 + \frac{1}{2} J_H \dot{\Theta}^2 - \frac{1}{2}\int_L EI\left(\frac{d^2 w}{dx^2}\right)^2 dx + W. \qquad (8)$$

Then, by noting that

$$J = \int_L \rho A x^2\, dx \qquad (9)$$

is the moment of inertia of the beam about the motor axis, and by recalling (4) and introducing the parametric transformation (see (3)), the Lagrangian may be shown to take the form

$$\mathcal{L} = \sum_{n=1}^{N}\left[\frac{1}{2}\rho_n A_n l_n \int_0^1 \{\dot{Q}_n\}^T [\Phi]^T [\Phi]\{\dot{Q}_n\}\, ds + \frac{1}{2} m_T \dot{w}_N^2 + \rho_n A_n l_n \int_0^1 \dot{\Theta}(x_{n-1} + l_n s)[\Phi]\{\dot{Q}_n\}\, ds + m_T L \dot{\Theta}\dot{w}_N + \frac{1}{2}(J_H + J)\dot{\Theta}^2 + \frac{1}{2} m_T L^2 \dot{\Theta}^2 - \frac{1}{2}\frac{EI}{l_n^3}\int_0^1 \{Q_n\}^T \left[\frac{d^2\Phi_n}{ds^2}\right]^T \left[\frac{d^2\Phi_n}{ds^2}\right]\{Q_n\}\, ds + W\right]. \qquad (10)$$

This expression is used in (6) where the q_i are taken as $q_i \in \{\Theta, \{Q\}\}$. On an element-by-element basis, each term of the Lagrangian will contribute to the equations of motion in the following way.

On the right-hand side of (10), each n yields individual element mass and stiffness matrices as well as consistent force vectors. These assemble into the global equations in the usual way except that it must be noted that Θ appears as a degree of freedom in all the element-level matrices.

The global mass matrix can be represented as

$$[M] = \begin{bmatrix} M_{JJ} & M_{JB} \\ M_{JB}^T & M_{BB} \end{bmatrix} \qquad (11)$$

where $[M_{BB}]$ is associated with the elastic degrees of freedom, M_{JB} represents the coupling between these elastic degrees of freedom and Θ, and M_{JJ} is the total rotary inertia of the system about the motor axis.

In (10) the first six terms on the right-hand side contribute solely to the global mass matrix, each group of six terms in the summation providing an individual element mass matrix. The first and second terms will contribute to the submatrix M_{BB} while the third and fourth terms contribute to the coupling matrix M_{JB}. The fifth and sixth terms give rise to the contributions of the beam, the hub, and the tip mass to the rotary inertia of the apparatus about the motor axis, and they contribute to the 1×1 submatrix M_{JJ}.

The global stiffness matrix is obtained from the penultimate term in (10) with each value of n yielding an individual element stiff matrix.

The global stiffness matrix will have the form

$$[K] = \begin{bmatrix} 0 & 0 \\ 0 & K_{BB} \end{bmatrix} \qquad (12)$$

where $\{K_{BB}\}$ is associated with the elastic degrees of freedom. Note that the elastic degrees of freedom do not couple with Θ through the stiffness matrix. A more detailed discussion of the derivation and form of the element mass and stiffness matrices may be found in Chapnik [26].

The last term in the expression for $\mathcal{L}$ (see (10)) yields the consistent force vector $\{F\}$.

The global damping matrix has the form

$$[C] = \begin{bmatrix} F_v & 0 \\ 0 & C_{BB} \end{bmatrix} \qquad (13)$$

where $[C_{BB}]$ denotes the submatrix associated with the material damping. The matrix $[C_{BB}]$ is obtained by assuming, for the reasons stated in the introduction to the development of the finite-element model, that the beam exhibits characteristic Rayleigh damping (i.e., $[C_{BB}] = b_1[M_{BB}] + b_2[K_{BB}]$). The assumption of Rayleigh damping dictates that

$$b_1 = \frac{2\omega_1\omega_2(\xi_1\omega_2 - \xi_2\omega_1)}{\omega_2^2 - \omega_1^2} \qquad b_2 = \frac{2(\xi_2\omega_2 - \xi_1\omega_1)}{\omega_2^2 - \omega_1^2} \qquad (14)$$

where ξ_n, $n = 1, 2$ is the damping coefficient of the nth mode and ω_n, $n = 1, 2$ is the natural frequency of the nth

mode. The constants of proportionality, b_1 and b_2, are found using the damping coefficients and natural frequencies for the first two vibrational modes (where the second mode is, of course, damped more than the first mode). The natural frequencies are found by solving the eigenvalue problem, i.e., finding the values of ω^2 for which $[K] - \omega^2[M] = 0$. These natural frequencies will, of course, be dependent on the boundary conditions imposed on the mass and stiffness matrices. It is worth mentioning that the case where the natural frequency is zero corresponds to the rigid body component of the motion, which sometimes requires special attention when designing a control strategy [22]. Since the arm is alternately slipping or sticking (see Section IV), two different sets of boundary conditions are used ($w_0 = \theta_0 = 0$ when the hub is slipping $w_0 = \theta_0 = \Theta = 0$ when it is sticking), leading to two sets of natural frequencies and thus two different global damping matrices.

In order to incorporate viscous friction effects on the hub into the model, an experimentally determined constant of viscous hub friction (F_v) is included in the (1, 1) entry of the damping matrix (i.e., that entry associated with Θ). Since viscous hub friction does not in any way affect the Rayleigh damping in the beam material, the first row and column of $[C]$ must otherwise be zero.

Note that hub friction is *not* modeled as additional hub inertia, a technique used by other researchers [23] when simplifying equations based on modal analysis.

IV. Modeling Friction

Any motor dynamics contributing to energy loss in the system, including electromagnetic effects, are included by modeling them as friction. Friction inherent in the hub (due to rotor characteristics, imperfectly aligned motor shaft, electromagnetic effects, etc.) is modeled as a combination of Coulomb and viscous friction.

The static Coulomb friction values used in the simulation were obtained experimentally by determining the torque required to move the beam from rest at various values of Θ, applying step torques of different amplitudes. In this way, a mean value of static Coulomb friction was obtained that represented the torque threshold required for hub motion. In our experimental apparatus, this mean value varied significantly depending on the sign of the applied torque. In other words, it required more torque to move the beam in one direction than in the other (see Table I). This is likely due to both imperfect shaft alignment and alignment of the rotor brushes. Thus, there are two appropriate values of static Coulomb friction, the relevant value at any given time depending on the sign of the velocity of the hub.

Using the measured value of static friction at the rest position ($\Theta = 0$) of the arm as a threshold for hub motion (i.e., the stick → slip boundary), the beam motion was simulated using (5) with the hub clamped by introducing the boundary condition $\Theta(t) = 0$, $t < t_{\text{slip}}$. When the bending moment about the hub axis exceeds the static friction torque threshold (which in turn depends on the sign of the moment about the hub), this boundary condition is removed, allowing rotation of the hub and arm.

TABLE I
Summary of Model Parameters

L (Effective Beam Length)	0.7652 m
E (Young's Modulus)	6.5×10^{10} Pa
I (Second Moment of the Area)	35.5185×10^{-12} m^4
A (Beam Cross-Sectional Area)	103.23×10^{-6} m
M_{beam} (Beam Mass)	0.2022 kg
M_{tip} (Payload Mass)	0.153 kg
m_{ball} (Mass of Impacting Sphere)	0.0795 kg
ξ_1 (First-Mode Damping Coefficient)	0.001
ξ_2 (Second-Mode Damping Coefficient)	0.003
ξ_3 (Third-Mode Damping Coefficient)	0.007
q_k (Geometric Impact Parameter)	0.343
A (Geometric Impact Parameter)	42.2 m^{-1}
B (Geometric Impact Parameter)	104.7 m^{-1}
δ_1 (Material Impact Parameter)	18.8×10^{-12}
δ_2 (Material Impact Parameter)	1.4×10^{-12}
F_{s_1} (Static Coulomb Friction Torque)	0.059 Nm
F_{s_2} (Static Coulomb Friction Torque)	−0.037 Nm
F_v (Viscous Friction Coefficient)	0.002 Nms
$K.E._{\text{stick}}$ (K.E. Stick Threshold)	10^{-5} J
$\lvert\dot{\Theta}\rvert_{\text{stick}}$ (Hub Speed Stick Threshold)	5.0×10^{-4} rad/s

A standard dynamic Coulomb friction model was adopted, where the friction force opposes the hub velocity. It was determined that the best estimate of the magnitude of the opposing dynamic friction force was equal to that of the static friction force acting in that direction. Mathematically,

$$\begin{aligned} F_{dc} &= F_{s_1}, \qquad \dot{\Theta} < 0 \\ &= F_{s_2}, \qquad \dot{\Theta} \geq 0 \end{aligned} \tag{15}$$

where F_{s_1} and F_{s_2} are the two limits of static Coulomb friction, and F_{dc} is the dynamic Coulomb friction. Once determined, F_{dc} is incorporated into the simulation by including it in the first entry in the applied force vector in (5).

Traversal of the slip → stick boundary is determined by the hub speed and the kinetic energy in the beam. When these variables fall simultaneously beneath experimentally determined thresholds ($K.E._{\text{stick}}$ and $\lvert\dot{\Theta}\rvert_{\text{stick}}$), the hub "clamps" again (the boundary condition is reintroduced as $\Theta(t) = \Theta_{\text{boundary}}$), not to slip again until the bending moment about the hub axis again exceeds the static friction threshold. Examination of the kinetic energy in the beam is required in order to prevent the hub from sticking, due to momentarily low hub speeds, while the mass center of the beam swings through the rigid-body line (i.e., when the hub velocity switches sign). The beam kinetic energy is obtained using

$$K.E._{\text{beam}} = \frac{1}{2}\{\dot{Q}^*\}^T[M_{BB}]\{\dot{Q}^*\} \tag{16}$$

where $\{Q^*\} = [w_0, \theta_0, w_1, \theta_1, \cdots, w_N, \theta_N]^T$.

The slip-stick boundary negotiation, as described here, has been used (albeit in a simpler form) by others to model slip-stick behavior in translational vibratory systems [24].

Viscous hub friction (F_v) was found to be relatively constant over the range of velocities encountered in the experiments. The value used in the simulations was obtained by simulating arm responses to many different velocity impacts and comparing simulation results to experimental data. It was found that higher values of F_v tend to increase the modal

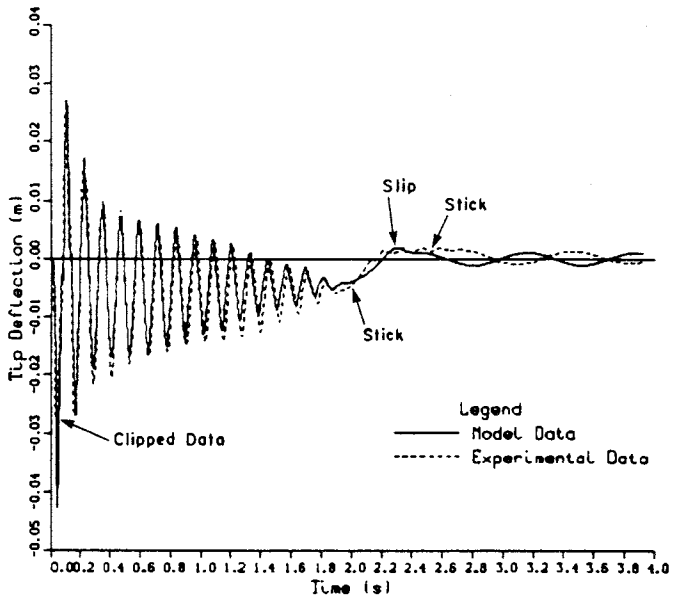

Fig. 3. Vibrational response for −1.95-m/s impact.

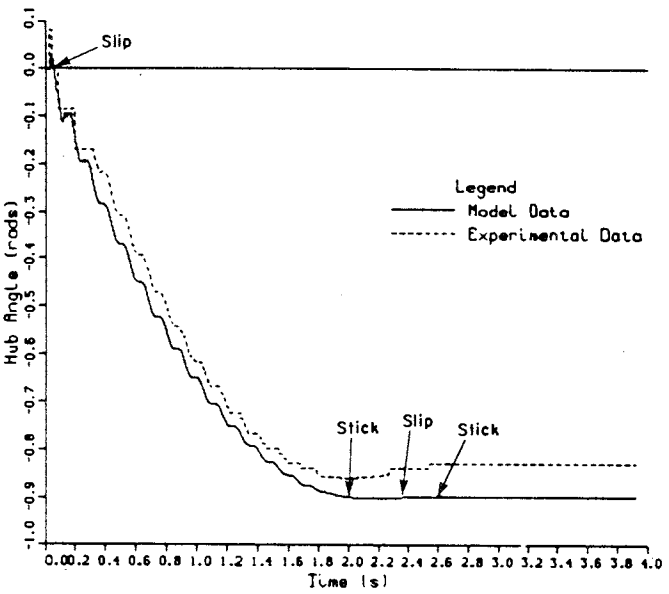

Fig. 4. Hub response for −1.95-m/s impact.

decay rates for all modes of vibration. Figs. 9 and 10 (which are discussed in more detail later) show the effect of quadrupling F_v to 0.008 from the tabular value of 0.002 (Figs. 3 and 4).

The friction model derived in this section is relatively simple and considers only the case where no hub torques are being applied. In the presence of applied hub torques, the motor will respond differently to externally applied torques, as its internal electromagnetic charateristics will be different. It must be noted that, in spite of the simplicity of the friction model employed here, excellent agreement with experimental results was obtained. Frictional effects must be taken into account in some manner for the model results to agree with experimental data.

V. Incorporation of Impact Load into the Model

The energy transferred to the flexible arm via impact must be represented in the finite-element formulation by the initial conditions on the displacement and velocity, and for purposes of solution, on the acceleration. In order to define these initial conditions, the motion of the beam after impact will be formulated analytically.

Following impact, the beam deflection can be represented by

$$w(x,t) = \sum_{n=1}^{\infty} u_n(x) C_n(t), \qquad x \in [0, L],\ t \in [0, \infty) \tag{17}$$

where $u_n(x)$ are characteristic functions normalized according to

$$\int_0^L \left[u_n(x)\right]^2 dx = 1 \tag{18}$$

and $C_n(t)$ are time-dependent modal coordinates. In this analysis, it is assumed that the hub remains clamped for the duration of the impact. This is a reasonable assumption for the experimental configuration and range of impact velocities considered in this investigation because static friction in the hub must be overcome before the hub can rotate, and this takes significantly more time than the impact contact duration. Thus, $u_n(x)$ describes the mode shapes of a clamped-free beam [25]:

$$u_n(x) = Q_n\left[\cos(\beta_n x) - \cosh(\beta_n x) - \alpha_n(\sin(\beta_n x) - \sinh(\beta_n x))\right] = Q_n \Psi_n(x) \tag{19}$$

where

$$\beta_n = \left[\frac{\omega_n^2 \rho A}{EI}\right]^{1/4}$$

$$\alpha_n = \frac{\cos(\beta_n L) + \cosh(\beta_n L)}{\sin(\beta_n L) + \sinh(\beta_n L)}$$

and

$$Q_n = \left(\int_0^L \left[\Psi_n(x)\right]^2 dx\right)^{-1/2}.$$

Note that the mode shapes for a clamped-free beam with and without tip mass are identical [26] but the addition of the tip mass causes the natural frequencies of vibration to change. The frequencies are given by the roots of the following frequency equation in β_n (which depends on ω_n):

$$1 + \cosh(\beta_n L)\cos(\beta_n L) + \beta_n L \frac{M_{\text{tip}}}{M_{\text{beam}}}(\sinh(\beta_n L) \cdot \cos(\beta_n L) - \sin(\beta_n L)\cosh(\beta_n L)) = 0. \tag{20}$$

The time-varying modal coordinates produced in a damped beam due to a force $F(t)$ applied at its tip ($x = L$) are given by the solution of

$$\frac{d^2 C_n(t)}{dt^2} + 2\xi_n \omega_n \frac{dC_n(t)}{dt} + \omega_n^2 C_n(t) = \frac{F(t) u_n(L)}{\rho A}. \tag{21}$$

Assuming that the beam is stationary at $t = 0$ (i.e., $C_n(0) = \dot{C}_n(0) = 0$), then

$$C_n(t) = \frac{u_n(L)}{\omega_{dn} q} \int_0^T \sin\left(\omega_{dn}(t-\tau)\right) e^{-\xi_n \omega_n (t-\tau)} F(\tau)\, d\tau \tag{22}$$

where q is the mass of the beam per unit length, ω_{dn} is the nth damped natural frequency, and $T = 1.0873 T_{MH}$, T_{MH} being the Hertz contact time (the duration of impact for two colliding bodies [8]), modified to account for beam vibration. This modification is accomplished [18] by regarding the impact as being not just between the beam (including tip mass) and the lead sphere, but between the beam (including tip mass) and an equivalent mass M_e given by

$$\frac{1}{M_e} = \frac{1}{m_{\text{ball}}} + \frac{1}{M_1} \tag{23}$$

where $M_1 = \rho A / (u_1(L))^2$ is the reduced mass of the first mode of the beam. The Hertz contact time is then given by [8]

$$T_{MH} = \frac{2.9432}{v_0^{1/5}} \left(\frac{5}{4 k_1 k_2} \right)^{2/5} \tag{24}$$

where

$$k_1 = \frac{M_e + (M_{\text{beam}} + M_{\text{tip}})}{M_e (M_{\text{beam}} + M_{\text{tip}})}$$

$$k_2 = \frac{4}{3} q_k / \left(\sqrt{A + B} \left(\delta_1 + \delta_2 \right) \right).$$

The variables q_k, A, B, δ_1, and δ_2 depend on the geometry and material properties of the colliding objects, as discussed by Goldsmith [8]. For our experimental apparatus, the numerical values of these parameters are listed in Table I.

The above expression (see (22)) for $C_n(t)$ can be calculated if $F(t)$ is known. An approximate contact force function, sufficient to predict the response of the beam after impact, is given by

$$F(t) = m v_0 (1 + e) \left(\frac{1 - \cos\left(\frac{2\pi t}{T} \right)}{T} \right), \qquad 0 \le t \le T \tag{25}$$

where m is the mass of the impacting sphere, v_0 is its velocity prior to impact, and e is the coefficient of restitution for the impact. Note that this coefficient of restitution depends on the dynamic response of the beam during impact. A force variation similar to the one used here, but shifted such that its maximum value occurs at $t = 0$, has previously been described as being close to the actual force variation [8], [17], [18].

Substituting (25) into (22) and making the assumption that

$$w_{dn} T \ll 1 \tag{26}$$

yields the modal coordinates for impact loading. Specifically,

$$C_n(t) = \frac{m v_0 (1 + e) u_n(L) \left(\frac{2\pi}{T} \right)^2 e^{-\xi_n \omega_n t} \left[K_1 \sin(\omega_{dn} t) - K_2 \cos(\omega_{dn} t) \right]}{q \omega_n^2 d_1 d_2} \tag{27}$$

where

$$K_1 = \omega_{dn} \left((2\xi_n \omega_n)^2 - \omega_n^2 + \left(\frac{2\pi}{T} \right)^2 \right)$$

$$K_2 = \xi_n \omega_n \left((2\xi_n \omega_n)^2 - 3\omega_n^2 + \left(\frac{2\pi}{T} \right)^2 \right)$$

$$d_1 = (\xi_n \omega_n)^2 + \left(\omega_{dn} - \frac{2\pi}{T} \right)^2$$

$$d_2 = (\xi_n \omega_n)^2 + \left(\omega_{dn} + \frac{2\pi}{T} \right)^2.$$

Every quantity in $C_n(t)$ is known except for the coefficient of restitution e, which will be found using energy conservation principles.

Note that the approximation given in (26) is valid only if ω_{dn} is small. Because higher modes of vibration have smaller values of the modal coordinates (due to the decaying exponential in the numerator and the ω_n^2 in the denominator), which makes their contribution to the overall response increasingly insignificant, modes higher than the third will be disregarded in the analysis (i.e., (17) is modified to sum only over $n = 1, 2, 3$). For the experimental apparatus used here, the product $\omega_{dn} T$ is sufficiently small for the first three modes of vibration to satisfy the approximation in (26). However, it must be realized that in making this approximation and in truncating the series to include only the first three modes, minor modeling errors are introduced.

In order to determine the coefficient of restitution, consider the following. The energy absorbed from the impact by each of the modes of vibration can be divided into beam potential energy, beam kinetic energy, and the kinetic energy of the tip mass. At $t = T$, for each mode, these can be represented by

$$P.E._n^{\text{beam}}(T) = \frac{1}{2} EI \int_0^L \left[u_n''(x) C_n(T) \right]^2 dx$$

$$K.E._n^{\text{beam}}(T) = \frac{1}{2} \rho A \int_0^L \left[u_n(x) \dot{C}_n(T) \right]^2 dx$$

$$K.E._n^{\text{tip mass}}(T) = \frac{1}{2} m_{\text{tip}} \left[u_n(L) \dot{C}_n(T) \right]^2. \tag{28}$$

The three energy terms can now be combined to represent

TABLE II
SUMMARY OF IMPACT PARAMETERS

	$v_0 = -1.60$ m/s	$v_0 = -1.95$ m/s
T_{MH}	0.18053 ms	0.17353 ms
e	0.763603	0.763606
C_1	5.799×10^{-5} m$^{3/2}$	6.41682×10^{-5} m$^{3/2}$
C_2	-4.34599×10^{-5} m$^{3/2}$	-5.04518×10^{-5} m$^{3/2}$
C_3	3.25244×10^{-5} m$^{3/2}$	3.7856×10^{-5} m$^{3/2}$
$\dot{C}_1$	0.701175 m$^{3/2}$/s	0.854559 m$^{3/2}$/s
$\dot{C}_2$	-0.27101 m$^{3/2}$/s	-0.330293 m$^{3/2}$/s
$\dot{C}_3$	0.192119 m$^{3/2}$/s	0.234144 m$^{3/2}$/s

the total energy in each mode after impact:

$$\Delta E_n(T) = P.E._n^{\text{beam}}(T) + K.E._n^{\text{beam}}(T) + K.E._n^{\text{tip mass}}(T) \tag{29}$$

from which the total energy in the flexible-arm system after impact can be obtained by summing over the modes [18]:

$$\Delta E(T) = \sum_{n=1}^{3} \Delta E_n(T) = \frac{1}{2} m v_0^2 (1+e)^2 R = E(1+e)^2 R \tag{30}$$

where E is the kinetic energy of the impacting sphere before impact and R represents the sum of modal energies with the common factor $\frac{1}{2}mv_0^2(1+e)^2$ removed.

Since energy is assumed to be conserved during the impact, $\Delta E(T)$ also represents the energy lost by the impacting sphere. As the rebound velocity of the sphere is ev_0, this yields

$$\Delta E(T) = E(1 - e^2). \tag{31}$$

Equating (30) with (31) yields the coefficient of restitution for the impact:

$$e = \frac{1-R}{1+R}. \tag{32}$$

The terms $C_n(T)$ and $\dot{C}_n(T)$ are now completely determined from (27) and its derivative, and the initial conditions on the displacement and velocity vectors are given by (for each nodal location $0 \le x \le L$):

$$w(x,T) = \sum_{n=1}^{3} u_n(x) C_n(T), \qquad \dot{w}(x,T) = \sum_{n=1}^{3} u_n(x) \dot{C}_n(T),$$

$$\theta(x,T) = \sum_{n=1}^{3} u_{n,x}(x) C_n(T), \qquad \dot{\theta}(x,T) = \sum_{n=1}^{3} u_{n,x}(x) \dot{C}_n(T). \tag{33}$$

Note that $\Theta(T) = \dot{\Theta}(T) = 0$ since the hub is considered clamped at $t = T$. The values of $C_n(T)$ and $\dot{C}_n(T)$ ($n = 1, 2, 3$), the Hertz contact time and the coefficient of restitution are given in Table II. It is apparent from these data that the deflection of the beam at the end of the impact is very small and could probably have been ignored for the impact velocities used in the examples presented here. However, in the most general situation, the nonzero initial deflection must be included for completeness.

The acceleration vector is then derived from the displacement and velocity vectors according to (5), which must also be satisfied at $t = T$. Note that, for the dynamic post-impact simulation, the time scale has been shifted such that the time origin coincides with the end of impact (i.e., $t' = t - T$).

It is important to realize that the value of the coefficient of restitution is not a constant but depends on the velocity of the impacting sphere and the flexibility of the beam as described above. This means that (25) cannot be used as a direct input to the finite-element model for all impact velocities. In order to treat the impact problem by the finite-element method, it would be necessary to create a detailed finite-element model of the sphere, the tip mass, and the beam at a discretization level appropriate for dealing with the impact problem. The structural dynamics present during the impact have characteristic frequencies that are much higher than those associated with the flexure of the beam. The equations of motion would have to be integrated with a time step size that reflected the presence of the important high-frequency components in the solution. This would result in a finite-element model with an enormous number of degrees of freedom and a very small time step size, resulting in tremendous solution complexity and cost. This is unwarranted in light of our ability to deal with the impact part of the response analytically and to use these results as input to a very modest finite-element model.

VI. TIME-DOMAIN RESPONSE CALCULATION

To calculate the time-domain response of the beam after impact, the Newmark-β integration scheme [27] was implemented, yielding the vectors $\{\ddot{Q}\}$, $\{\dot{Q}\}$, and $\{Q\}$ from (5) after every integration time step (referred to as the acceleration, velocity, and displacement vectors, respectively).

First, the initial conditions are set. The initial displacement, velocity, and acceleration vectors are determined as described in Section V.

The integration constants for the Newmark-β method (γ and β) are then chosen, as is a time step (Δt) for the time-domain simulation. The values $\gamma = 0.5$, $\beta = 0.25$ were chosen to eliminate any algorithmic damping by the integration algorithm and to insure stability and second-order accuracy [28]. The time step is chosen, using a rule of thumb [29], to be $\frac{1}{100}$ of the period of the lowest frequency in the model. These quantities define constants that are used to calculate the solution vectors $\{Q\}$, $\{\dot{Q}\}$, and $\{\ddot{Q}\}$ at each subsequent time step.

VII. SIMULATION RESULTS

The finite-element model described above was implemented in the "C" programming language on a DEC Microvax II. Some modules from the **eispack** and **linpack**

Fortran libraries were accessed to calculate eigenvalues and to solve systems of linear equations.

All results given here were calculated using a 15-element model. Above this number of elements, the results do not change appreciably, and the time required for simulation increases rapidly. Relevant physical parameters for the impact and the ensuing motion are given in Table II.

Young's modulus for the aluminum beam had to be lowered slightly (7%) from the generally accepted handbook value [30] in order for the model to reflect the observed frequency of vibration of the beam. It should be noted that others have also found discrepancies with Young's modulus when investigating vibrating beams [31], and have not explained the phenomenon satisfactorily.

A sufficiently small time increment must be chosen to ensure that the torque about the hub, when it is clamped, reaches the stick → slip boundary (or just above it) at a time increment boundary. If the time increment chosen is too large, the bending moment about the hub may pass the stick → slip boundary at some early time point within the increment, causing the torque about the hub to be excessive when finally detected at the end of the increment, and an unrealistic response prediction occurs. Similarly, if the time increment is too large, it may be difficult to obtain values of hub speed and beam kinetic energy which fall simultaneously within the required tolerances in order for the motion to revert from slipping to sticking.

As can be seen in Figs. 3-6, the calculated displacements, both hub angle and elastic deflection, agree closely with those found experimentally. The experimental vibration data are clipped at the range limits of the elastic deflection sensor (see Fig. 3), a condition that was not imposed on the model.

Figs. 3 and 4 have noted on them the relevant changes in the state of the hub. The hub switches almost immediately (t = 0.0176 s) from the initial clamped state to free rotation. The hub angle is slightly positive at the outset due to the magnitude of beam flexure near the hub compared to the magnitude of rotation due to hub slippage. Also note that, while the hub rotates freely, the model prediction of the decay of the dominant mode correlates closely with experiment. The hub sticks at t = 2.114 s, but the static friction threshold is soon reached and the hub slips again (t = 2.278 s), this time in the direction opposite to impact. Finally, the hub clamps (t = 2.408 s), and the dominant first mode of the clamped response can be seen at the end of Fig. 3. The area of greatest disagreement between the model and experiment is in the region between the times when the hub first sticks and the time when it finally clamps. This disagreement is due to nonlinear effects caused by the transition from the slip condition to the stick condition that are not included in the model.

Figs. 5 and 6 have the same features as Figs. 3 and 4, but they occur at different times due to a different impact velocity. The hub starts to rotate freely at t = 0.0176 s, sticks first at t = 1.741 s, slips again at t = 2.013 s, and finally clamps at t = 2.152 s.

The importance of including the Coulomb friction in the model may be seen in Figs. 7 and 8, which may be compared

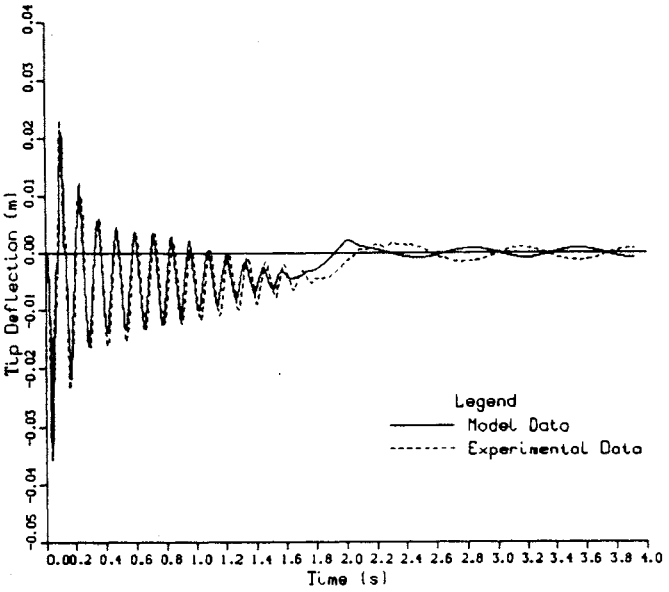

Fig. 5. Vibrational response for − 1.60-m/s impact.

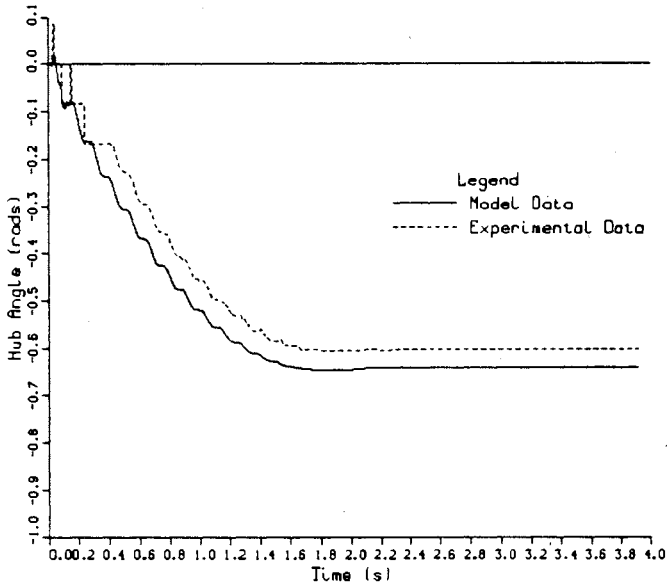

Fig. 6. Hub response for − 1.60-m/s impact.

with Figs. 3 and 4 to illustrate the response of the model when dynamic Coulomb friction is removed, although the slip-stick boundaries remain the same. Note especially the hub angle prediction, which increases almost linearly in the absence of any significant friction term to slow its progress. Since the hub velocity remains high, the slip → stick hub velocity threshold is never reached, and the beam never "clamps". Also note that the amplitude of vibration is much larger and that the oscillations are more symmetric about zero in the absence of dynamic Coulomb friction.

Figs 9 and 10 illustrate the effect of quadrupling the coefficient of viscous hub friction F_v from the value that gives the best agreement with experiment. When this change to the model is made, all of the modes, including the dominant first mode, decay more quickly than is evident in the experiment.

In conclusion, note especially the necessity of including all

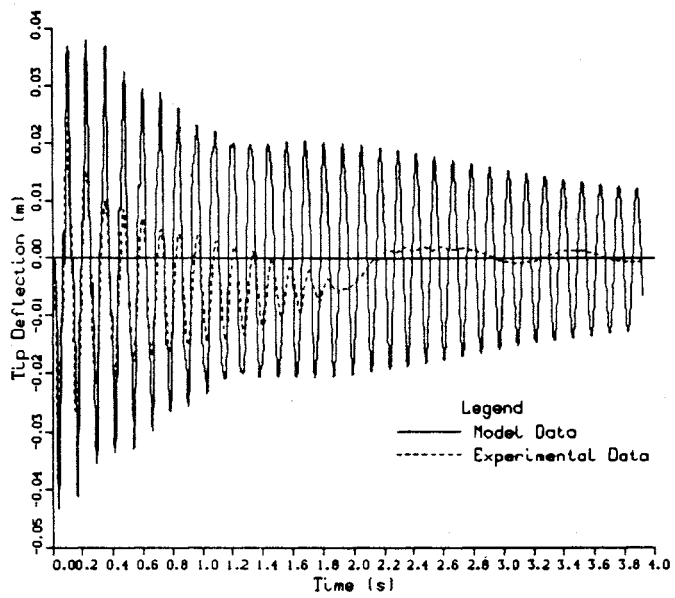

Fig. 7. Vibrational response without dynamic Coulomb friction. Impact velocity is -1.95 m/s.

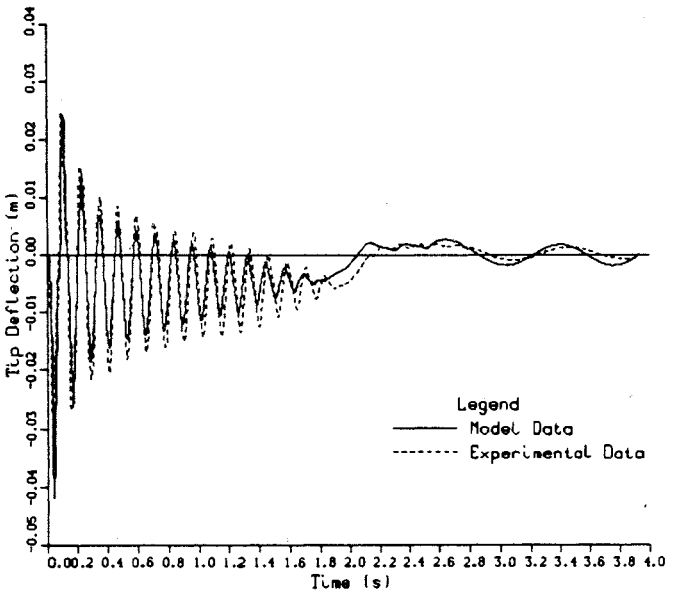

Fig. 9. Vibrational response ($w(L, t)$) with $F_v = 0.008$. Impact velocity is -1.95 m/s.

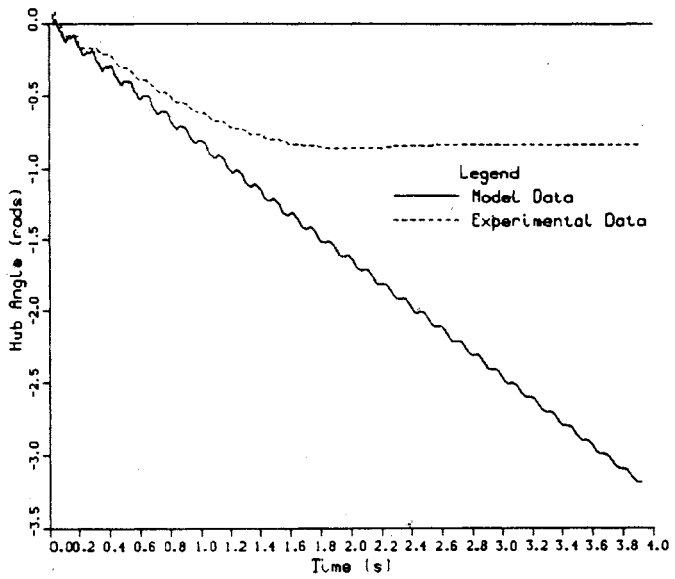

Fig. 8. Hub response without dynamic Coulomb friction. Impact velocity is -1.95 m/s.

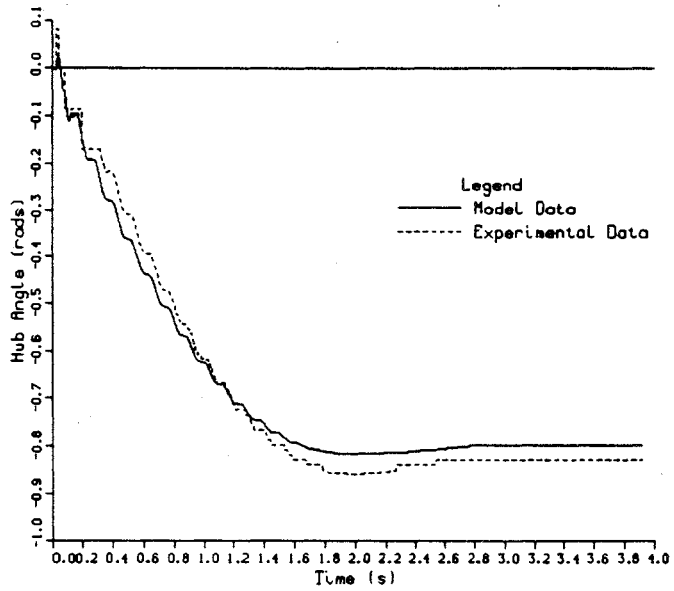

Fig. 10. Hub response ($\Theta(t)$) with $F_v = 0.008$. Impact velocity is -1.95 m/s.

of the frictional effects in the model to obtain good agreement with experiment.

VIII. Summary

From the experimental results, this enhanced finite-element model provides an accurate representation of the physical process being modeled. As well, the model provides a vehicle for investigating the effects of parameters of the process model, in particular, frictional effects and load profiles.

Impact loading has been effectively represented in terms of initial conditions and can be applied to a range of finite-element models in this manner. This class of model can aid the analysis of impact-induced structural vibrations, especially given the increasing popularity of the finite-element method for structural analysis and dynamic modeling.

Hub friction, both Coulomb and viscous, and Rayleigh beam damping have been introduced into this model of a single-link flexible robotic member. These effects have not been considered previously by most researchers in the field, particularly with respect to the consideration of slip–stick boundaries. Incorporation of these effects have the potential to improve the results of model-reference control strategies applied to this type of problem.

The model is well suited to be a design aid, via simulation, for the assessment of control strategies that may subsequently be applied to the experimental apparatus for physical verification [33].

References

[1] W. B. Gevarter, "Basic relations for control of flexible vehicles," *AIAA J.*, vol. 8, no. 4, pp. 666–672, Apr. 1970.

[2] R. H. Cannon and E. Schmitz, "Initial experiments on the end-point control of a flexible one-link robot," *Int. J. Robotic Res.*, vol. 3, no. 3, pp. 62–75, Fall 1984.

[3] W. J. Book, "Recursive Lagrangian dynamics of flexible manipulator arms," *Int. J. Robotics Res.*, vol. 3, no. 3, pp. 87-101, Fall 1984.
[4] W. J. Book and G. G.Hastings, "A linear dynamic model for flexible robotic manipulators," *IEEE Control Syst. Mag.*, vol. 7, no. 1, pp. 61-64, Feb. 1987.
[5] D. Wang and M. Vidyasagar, "Control of a flexible beam for optimum step response," in *Proc. IEEE Int. Conf. Robotics Automat.*, Apr. 1987, pp. 1567-1572.
[6] M. Balas and D. Meldrum, "Application of model reference adaptive control to a flexible remote manipulator arm," in *Proc. Amer. Control Conf.*, 1985, pp. 825-832.
[7] S. Timoshenko, *Vibration Problems in Engineering*. Princeton, NJ: D. Van Nostrand, 1955.
[8] W. Goldsmith, *Impact*. London: Edward Arnold Ltd., 1960.
[9] E. Bayo, "A finite-element approach to control the end-point motion of a single-link flexible robot," *J. Robotic Syst.*, vol. 4, no. 1, pp. 63-75, Winter 1987.
[10] ——, "Computed torque for the position control of open chain flexible robots," in *Proc. IEEE Int. Conf. Robotics Automat.*, Apr. 1988, pp. 316-321.
[11] C. H. Menq and J. S. Chen, "Dynamic modeling and payload-adaptive control of a flexible manipulator," in *Proc. IEEE Int. Conf. Robotics Automat.*, Apr. 1988, pp. 488-493.
[12] T. R. Kane and R. R. Ryan, "Dynamics of a cantilever beam attached to a moving base," *J. Guidance*, vol. 10, no. 2, pp. 139-151, Mar.-Apr. 1987.
[13] I. Sharf and G. M. T. D'Eleuterio, "Computer simulation of elastic chains using a recursive formulation," in *Proc. IEEE Int. Conf. Robotics Automat.*, Apr. 1988, pp. 1539-1545.
[14] G. B. Sincarsin and P. C. Hughes, "Dynamics of an elastic multibody chain: Part A—Body motion equations," *Dynamics, Stability Syst.*, vol. 4, nos. 3 and 4, 1989, pp. 209-226.
[15] P. C. Hughes and G. B. Sincarsin, "Dynamics of an elastic multibody chain: Part B—Global dynamics," *Dynamics Stability Syst.*, vol. 4, nos. 3 and 4, pp. 227-244, 1989.
[16] H. L. Mason, "Impact on beams," *J. Appl. Mechanics*, vol. 3, pp. A55-A61, 1936.
[17] C. Zener and H. Feshbach, "A method of calculating energy losses during impact,' *J. Appl. Mechanics*, vol. 6, pp. A67-A70, June 1939.
[18] E. H. Lee, "The impact of a mass striking a beam," *J. Appl. Mechanics*, vol. 7, pp. A129-A138, Dec. 1940.
[19] R. Deacon, "Design and control of a simple-link flexible robotic arm experiment," M.A.Sc. thesis, Univ. of Waterloo, Waterloo, Int., Canada, Winter 1988.
[20] R. A. Deacon, W. J. Wilson, and R. S. Ramshaw, "Control of a single-link flexible arm experiment," in *Proc. Can. Conf. Electrical Computer Eng.* (Vancouver, B.C., Canada, Nov. 3-4, 1988), pp. 606-610.
[21] ——, "A flexible robot arm LED precision position sensor," in *Proc. Conf. Electrical Computer Eng.* (Vancouver, B.C., Canada, Nov. 3-4, 1988), pp. 723-726.
[22] E. Bayo, P. Papadopoulos, J. Stubbe, and M. A. Serna, "Inverse dynamics and kinematics of multilink elastic robots," *Int. J. Robotics Res.*, vol. 8, no. 6, pp. 49-62, Dec. 1989.
[23] W. J. Book and G. G. Hastings, "Verification of a linear dynamic model for flexible robotic manipulators," in *Proc. IEEE Int. Conf. Robotics Automat.*, vol. 2, Spring 1986, pp. 1024-1029.
[24] P. Vielsack, "Sensitivity of clamp joints," *J. Dynamics Stability Syst.*, vol. 2, no. 2, pp. 139-147, 1987.
[25] E. Volterra and E. C. Zachmanoglou, *Dynamics of Vibrations*. Columbus, OH: Charles Merrill, 1965.
[26] B. V. Chapnik, "Modeling and control of impact on a one-link flexible robotic arm," M.A.Sc. thesis, Univ. of Waterloo, Waterloo, Ont., Canada, Fall 1989.
[27] K. J. Bathe, *Finite Element Procedures in Engineering Analysis*. Englewood Cliffs, NJ: Prentice-Hall, 1982.
[28] G. R. Heppler and J. S. Hansen, "Time integration of the equations of motion of a structural system including damping," *AIAA J.*, vol. 21, no. 9, pp. 1301-1309, Sept. 1983.
[29] D. R. J. Owen and E. Hinton, *Finite Elements in Plasticity: Theory & Practice*. Swansea, U.K.: Pineridge Press, 1980.
[30] *Metallic Materials and Elements for Aerospace Vehicle Structures*, U.S. Dept. of Defense, Mil-HDBK-5C, 1978.
[31] A. H. Von Flotow and B. Schafer, "Wave-absorbing controllers for a flexible beam," *J. Guidance*, vol. 9, no. 6, pp. 673-680, Nov.-Dec. 1986.
[32] T. K. Caughey, "Classical normal modes in damped linear dynamic systems," *J. Appl. Mechanics*, pp. 269-271, June 1960.
[33] B. V. Chapnik, G. R. Heppler, and J. D. Aplevich, "Controlling the impact response of a one-link flexible robotic arm," in *Proc. IEEE Int. Conf. Robotics Automat.*, vol. 2 (Cincinnati, OH), May 1990, pp. 1444-1449.

B. V. Chapnik, (S'88-M'89) received the B.A.Sc. and M.A.Sc. degrees in systems design engineering from the University of Waterloo, Waterloo, Ont., Canada, in 1988 and 1990, respectively.

He is presently a Staff Engineer with Vibron Limited and works on contracts related to vibrations, acoustics, and noise control.

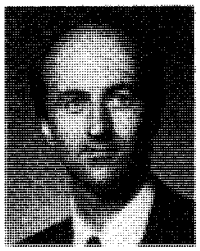

G. R. Heppler received the B.A.Sc. degree in aerospace engineering from the University of Toronto, Toronto, Ont., Canada, in 1977 and the M.A.Sc. and Ph.D. degrees in aerospace engineering from the University of Toronto Institute for Aerospace Studies in 1979 and 1985, respectively.

He worked for a year and a half with Boeing between graduate degrees. He has been an Assistant Professor in the Department of Systems Design Engineering at the University of Waterloo, Waterloo, Ont., since 1986. His research interests include structural dynamics and control and issues related to finite-element methods.

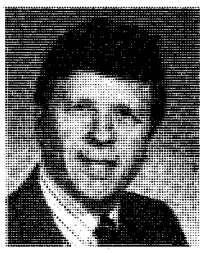

J. D. Aplevich received the B.E. degree from the University of Saskatchewan, Saskatoon, Sask., Canada, in 1964 and the Ph.D. degree from Imperial College, London, England, in 1968.

Following two years in the Committee on Mathematical Biology, University of Chicago, he moved to the University of Waterloo, Waterloo, Ont., where he has taught a variety of electrical and control subjects and held a variety of administrative positions, and where he is currently Professor of Electrical and Computer Engineering. He has held visiting academic positions at Imperial College, Université Paul Sabatier, Lund University, the Ecole Polytechnique de Montréal, and the University of Texas, Arlington. His interests include theory and applications of implicit system models, identification, computational aspects of control theory, and applications.